GA–A24788

HIGH PERFORMANCE INTEGRATED PLASMA CONTROL IN DIII–D

by
D.A. HUMPHREYS, R.D. DERANIAN, J.R. FERRON, R.J. JAYAKUMAR,
R.D. JOHNSON, R.R. KHAYRUTDINOV, R.J. LA HAYE, J.A. LEUER,
M.A. MAKOWSKI, B.G. PENAFLOR, M.L. WALKER, and A.S. WELANDER

AUGUST 2004

GENERAL ATOMICS

DISCLAIMER

GA–A24788

HIGH PERFORMANCE INTEGRATED PLASMA CONTROL IN DIII–D

by

D.A. HUMPHREYS, R.D. DERANIAN, J.R. FERRON, R.J. JAYAKUMAR,*
R.D. JOHNSON, R.R. KHAYRUTDINOV,† R.J. LA HAYE, J.A. LEUER,
M.A. MAKOWSKI,* B.G. PENAFLOR, M.L. WALKER, and A.S. WELANDER

This is a preprint of a paper to be presented at the 23rd Symposium on Fusion Technology, Venice, Italy, September 20–24, 2004 and to be published in the *Fusion Engineering and Design.*

*Lawrence Livermore National Laboratory, Livermore, California
†TRINITI Laboratory, Troitsk, Russia

Work supported by
the U.S. Department of Energy
under DE-FC02-04ER54698
and W-7405-ENG-48

GENERAL ATOMICS PROJECT 30200
AUGUST 2004

GENERAL ATOMICS

ABSTRACT

The DIII–D mission to explore the Advanced Tokamak (AT) regime places significant demands on the DIII–D plasma control system (PCS) [D.A. Humphreys, *et al.*, Fusion Eng. Des. **66–68**, 633 (2003)], including simultaneous and accurate regulation of plasma shape, stored energy, and density, as well as coordinated suppression of magnetohydrodynamic (MHD) instabilities. The present work describes selected new solutions to key control problems in DIII–D AT operation. These include novel nonrigid, resistive linear plasma response models, nonlinear algorithms for avoidance of current limiting, and improved NTM control algorithms.

1. INTRODUCTION

Plasma boundary control is complicated in DIII–D by the need to produce good performance in a wide range of shapes and configurations, as well as by a uniquely constrained poloidal field (PF) coil circuit and power supplies routinely operated near current limits [1]. Integrated plasma control methods using novel nonrigid, resistive linear plasma models for design of multivariable controllers, and nonlinear control algorithms to avoid current limiting effects have addressed this problem.

The integrated plasma control design approach was also key to achieving sustained suppression of both 3/2 and 2/1 NTM modes (separately) using the DIII–D electron cyclotron current drive (ECCD) system MW — to replace missing island bootstrap current [2]. We report on design and experimental use of new control algorithms using direct feedback on the q-profile, reconstructed with a realtime Grad-Shafranov calculation including motional Stark effect (MSE) measurements [3,4].

2. INTEGRATED PLASMA CONTROL

Integrated plasma control refers to an approach to plasma control design which makes use of validated plasma/system models for design of control algorithms, detailed simulations to confirm controller function, and connection of simulations to actual plasma control system (PCS) hardware and software to confirm performance and correctness of implementation. This process can provide high confidence, high reliability control while minimizing the use of machine time for experimental tuning. A suite of tools for applying this approach to tokamak controller design has been developed at DIII–D over the past decade, and has been applied to many devices in addition to DIII–D itself [5]. The DIII–D PCS supports this approach by allowing testing of control algorithms against simulations, as well as providing an architecture that supports real time use of many CPUs communicating on a fast network [6]. The DIII–D PCS has been adapted for use at NSTX and MAST, and is being adapted for use by KSTAR and EAST.

3. NONRIGID, RESISTIVE PLASMA RESPONSE MODELING

Although plasma response models that assume rigid vertical and radial displacements of the plasma have been successful in allowing predictive design of controllers, it has long been recognized that plasma shape responses are significantly nonrigid. Figure 1(a) shows such a plasma perturbation in DIII–D. Figure 1(b) shows that the amount each fluid element must be moved radially to produce the new current distribution varies across the midplane.

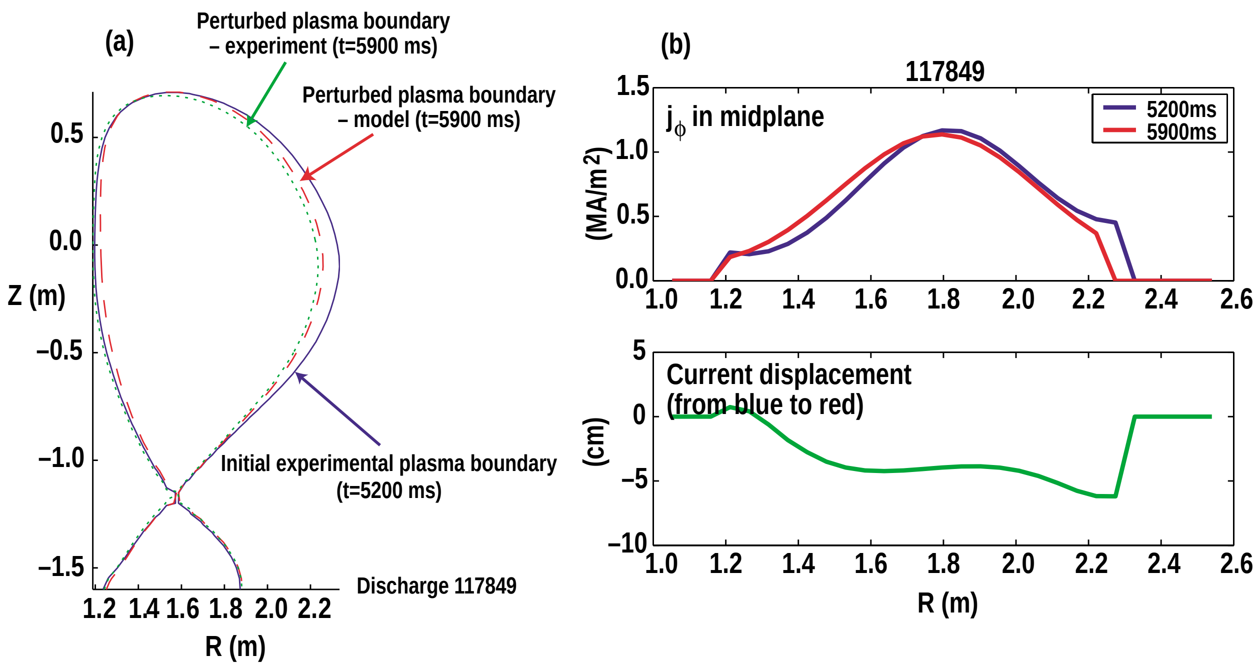

Fig. 1. Experimental DIII–D nonrigid plasma response corresponding to movement of outboard plasma boundary and no movement of inboard plasma boundary: (a) boundaries at two different times, before (solid) and after nonrigid displacement (dashed), as well as prediction of the displacement by a nonrigid plasma response model (dotted); (b) current profiles across midplane corresponding to the two times shown in (a) along with the local current element displacement required to match the observed profile change.

A nonrigid linear plasma response can be easily included in the axisymmetric MHD and circuit equations for all toroidal conductors (subscript "s") and all plasma fluid elements (subscript "p") [7]:

$$M_{ss}\dot{I}_s + R_{ss}I_s + M_{sp}\dot{I}_p + \frac{\partial\psi_s}{\partial\xi_R}\dot{\xi}_R + \frac{\partial\psi_s}{\partial\xi_Z}\dot{\xi}_Z = V_s \quad , \tag{1}$$

$$M_{pp}\dot{I}_p + R_{pp}I_p + M_{ps}\dot{I}_s + \frac{\partial\psi_p}{\partial\xi_R}\dot{\xi}_R + \frac{\partial\psi_p}{\partial\xi_Z}\dot{\xi}_Z = 0 \quad , \tag{2}$$

where I_{s} is the vector of perturbed conductor currents, I_{p} is the vector of perturbed plasma fluid element currents, V_{s} is the vector of perturbed conductor voltages, ψ_{s} is the vector of perturbed flux at conductors, ξ_{R} and ξ_{Z} are plasma fluid element major radial and vertical displacement vectors respectively, R denotes a resistance matrix, M denotes a mutual inductance matrix. The linearized radial (F_{R}) and vertical (F_{Z}) force balance at each (massless) fluid element are given respectively by

$$\delta F_{\mathrm{R}} = 0 = \frac{\partial F_{\mathrm{R}}}{\partial I_{\mathrm{s}}} I_{\mathrm{s}} + \frac{\partial F_{\mathrm{R}}}{\partial I_{\mathrm{p}}} I_{\mathrm{p}} + \frac{\partial F_{\mathrm{R}}}{\partial \xi_{\mathrm{R}}} \xi_{\mathrm{R}} + \frac{\partial F_{\mathrm{R}}}{\partial \xi_{\mathrm{z}}} \xi_{\mathrm{z}} + \frac{\partial F_{\mathrm{R}}}{\partial \beta_{\mathrm{p}}} \beta_{\mathrm{p}} \quad , \tag{3}$$

$$\delta F_{\mathrm{Z}} = 0 = \frac{\partial F_{\mathrm{Z}}}{\partial I_{\mathrm{s}}} I_{\mathrm{s}} + \frac{\partial F_{\mathrm{Z}}}{\partial I_{\mathrm{p}}} I_{\mathrm{p}} + \frac{\partial F_{\mathrm{Z}}}{\partial \xi_{\mathrm{R}}} \xi_{\mathrm{R}} + \frac{\partial F_{\mathrm{Z}}}{\partial \xi_{\mathrm{z}}} \xi_{\mathrm{z}} + \frac{\partial F_{\mathrm{Z}}}{\partial \beta_{\mathrm{p}}} \beta_{\mathrm{p}} \quad , \tag{4}$$

where β_{p} is a perturbed poloidal beta (scalar or vector representing local values). Eq. (2) allows each fluid element current to vary according to the local neoclassical resistivity and) accurately accounts for resistive magnetic flux diffusion through the plasma, provided the plasma resistivity is sufficiently well known.

Figure 1(a) compares the accurate prediction of the nonrigid plasma response model to the experimental change in the outer gap shown.

4. NONLINEAR CONTROL ALGORITHMS

Maximizing performance in a tokamak often leads to operation near or at power supply current limits. As in all tokamaks, coil current limits consistent with power supply requirements constrain the range of shapes that can be achieved in DIII–D. Figure 2 shows the currents in each coil that would be required to exactly satisfy a common DIII–D target shape. For several coils the required currents lie outside the allowed values indicated for DIII–D.

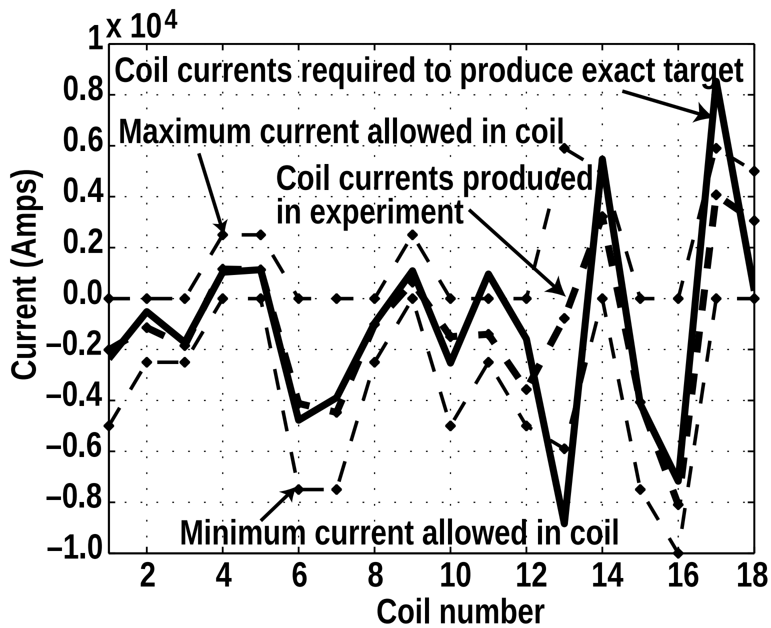

Fig. 2. Coil currents required to exactly achieve a common DIII–D equilibrium, range of allowable currents, and experimentally produced currents.

To avoid empirical tuning and improve control performance, the integrated plasma control approach is being used with the response models of Section 3 to predictively design linear multivariable controllers. However, when such linear controllers are used, they extend coil current demands to reduce errors to zero, even when currents are near limits. To avoid this, logic has been added to modify the error in order to prevent limiting [8]. Algorithms have also been developed to adaptively compute a nominal coil current trajectory vector to minimize the proximity to limits while maintaining good shape control. Coil current vectors in the "shape nullspace" of coil current vectors that do not (significantly) affect the plasma shape can be added to the equilibrium current vector to move it away from current limits.

We define I_{center} to be the vector of currents that are midway between the minimum and maximum allowed current values for each PF coil. Given a measured current I_{meas}, we wish to find a minimizing nominal current vector $I_{nom} = \arg\min_{I} \|W(I - I_{center})\|$ such that it produces the same error signal as I_{meas}. The weight W accounts for different allowable coil current ranges. This reduces to the optimization problem

$$\min_{q} \left\| W(P_{N^\perp}(I_{meas} - I_{center}) + X_N(q - q_{center})) \right\|^2 \quad , \tag{5}$$

where X_N is the matrix of orthonormal basis vectors for the shape nullspace N, $N^\perp$ refers to the current vector space which does affect the shape, $P_{N^\perp}$ is the projection onto $N^\perp$, q is the vector of coefficients of the shape nullspace basis vectors, and $q_{center} = X_N^T I_{center}$. Equation (5) has the solution $q = Q(I_{meas} - I_{center}) + q_{center}$ where $Q = -(WX_N)^\dagger WP_{N^\perp}$ where the dagger represents the pseudoinverse. Then $I_{nom} = P_{N^\perp} I_{meas} + X_N q$ is the desired nominal current.

Figure 3 illustrates this process in simulation for a single coil that tends to fall to a current level near zero (experimental current). The simulated current evolution approaches the current level midway between the maximum and minimum limits, increasing the headroom for current demands without changing the plasma shape.

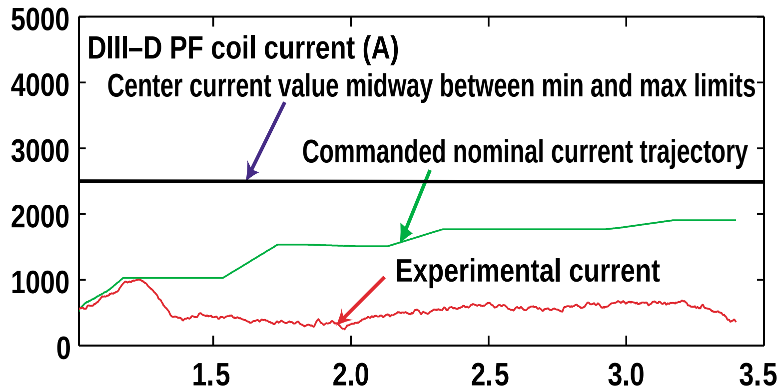

Fig. 3. Simulation illustrating calculation of desired current trajectory for a PF coil in DIII–D that frequently drifts to zero current. The commanded trajectory moves steadily toward the centered value of 2500 A.

5. REALTIME SAFETY FACTOR FEEDBACK FOR NTM SUPPRESSION

The "Search and Suppress" and "Active Tracking" algorithms for NTM control in DIII–D regulate the plasma major radius or the toroidal field in order to produce alignment of the island and ECCD deposition location. The Search and Suppress algorithm scans one of these control quantities in discrete steps, with pauses to assess the effect on the island size (inferred from the RMS amplitude of high frequency magnetic measurements). The optimal alignment can be determined by empirical scans of the control parameter, through predictive calculation of the deposition location with the GA-TORAY [9] code, or through Search and Suppress action. Successful suppression results in a freeze of the control quantity and an activation of the Active Tracking algorithm, which keeps the resonant surface at the location that produced mode suppression.

Recently the realtime equilibrium reconstruction algorithm (RTEFIT) [3] has been upgraded to provide realtime safety factor (q) calculation based on MSE and magnetic measurements [4]. The Active Tracking algorithm can now use the real time determination of the q-surface geometry to maintain alignment after the mode has been suppressed. Figure 4 shows results of a DIII–D experiment in which the plasma major radius was set at a previously determined location producing good initial island-ECCD alignment, and the 3/2 mode was prevented from growing as the beam power was increased [Fig. 4(a)]. Figure 4(c) shows that the new q-surface feedback algorithm successfully held the major radius of the 3/2 surface ($R_{q=3/2}$) at the deposition location (Target ECCD), fixed in the lab frame, by e changing the plasma major radius (R_{SURF}) several centimeters.

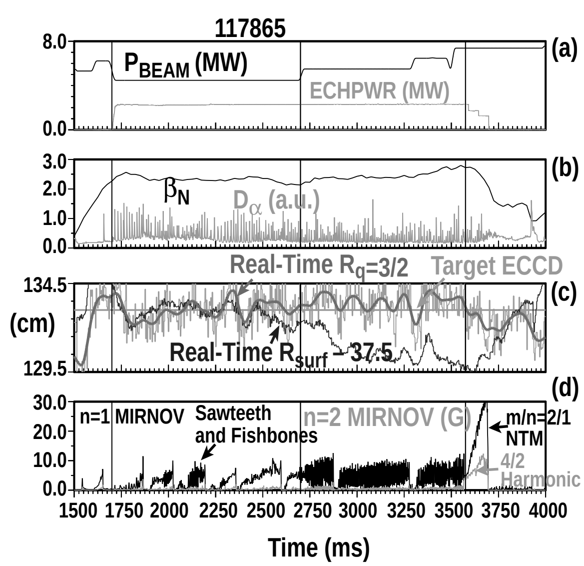

Fig. 4. DIII–D NTM suppression experiment demonstrating successful use of realtime q-surface reconstruction and feedback to prevent 3/2 NTM growth and maintain good island-ECCD alignment.

6. SUMMARY AND CONCLUSIONS

Integrated plasma control tools developed for DIII–D have enabled solutions for a wide variety of problems encountered in high performance operation. Recent progress in development of these control tools include nonrigid plasma response models for improved shape control, nonlinear control algorithms to avoid coil current limiting, and direct feedback on realtime q-surface reconstruction for improved NTM suppression. Detailed simulations using validated models have allowed testing and confirmation of control algorithms prior to experimental implementation, and minimized the need for experimental tuning. These tools can also be valuable in design and confirmation of control performance for next-generation devices.

REFERENCES

[1] M.L. Walker, *et al.*, Control of plasma poloidal shape and position in the DIII–D tokamak, Proc. 36th IEEE Conf. on Decision and Control, San Diego, CA (1997) 3703.

[2] R.J. La Haye, *et al.*, Control of neoclassical tearing modes in DIII–D, Phys. Plasmas **9** (2002) 2051.

[3] J.R. Ferron, *et al.*, Realtime equilibrium reconstruction for tokamak discharge control," Nucl. Fusion **38** (1998) 1055.

[4] B.W. Rice, *et al.*, Rev. Sci. Instrum. **70** (1999) 815

[5] J.A. Leuer, *et al.*, DIII–D integrated plasma control tools applied to next-generation Devices," these proceedings.

[6] B.G. Penaflor, *et al.*, Current status of DIII–D plasma control system computer upgrades, Proc. 4th IAEA Technical Meeting on Control, Data Acquisition and Remote Participation for Fusion Research, San Diego, California (2003) to appear in Fusion Eng. and Design.

[7] R. Albanese, *et al.,* Plasma modeling for vertical instabilities, Nucl. Fusion **29** (1989) 1013.

[8] M.L. Walker, et al., Some nonlinear controls for nonlinear processes in the DIII–D tokamak, Proc. 42nd IEEE Conf. on Decision and Control, Maui, Hawaii (2003) p. 6565.

[9] A.H. Kritz, *et al.*, Proc. 3rd International Symposium on Heating in Toroidal Plasmas, Grenoble, Italy (1982) (ECE, Brussels, 1982) Vol. 2, p. 707.

ACKNOWLEDGMENT

This is a report of work supported by the U.S. Department of Energy under Cooperative Agreement. DE-FC02-04ER54698 and W-7405-ENG-48.